A HIGH-RESOLUTION GE SPECTROMETER FOR GAMMA-RAY BURST ASTRONOMY

A. OWENS[1], R. BAKER, T. L. CLINE, N. GEHRELS, J. JERMAKIAN, T. NOLAN[2], R. RAMATY, H. SEIFERT[3], D. A. SHEPHARD[4], G. SMITH[5], D. E. STILWELL and B. J. TEEGARDEN
Laboratory for High Energy Astrophysics, NASA/Goddard Space Flight Center Greenbelt, MD 20771, U.S.A.

C. P. CORK, D. A. LANDIS, P. N. LUKE, N. W. MADDEN, D. MALONE, R. H. PEHL and H. YAVER
Lawrence, Berkeley Laboratory, Berkeley, CA 94702, U.S.A.

K. HURLEY
Space Sciences Laboratory, University of California, Berkeley, CA 94720, U.S.A.

and

S. MATHIAS and A. H. POST, JR.
Arthur D. Little Inc., Cambridge, MA 02140, U.S.A.

(Received 18 June, 1995)

Abstract. The Transient Gamma-Ray Spectrometer (TGRS) to be flown aboard the WIND spacecraft is primarily designed to perform high resolution spectroscopy of transient γ-ray events, such as cosmic γ-ray bursts and solar flares over the energy range 25 keV to 8.2 MeV with an expected spectroscopic resolution of $\sim$ 3 keV at 1 MeV. The detector itself consists of a 215 cm^3 high purity n-type Ge crystal kept at cryogenic temperatures by a passive radiative cooler. The geometric field of view defined by the cooler is $\sim 1.8\pi$ steradian. To avoid continuous triggers by soft solar events, a thin BeCu Sun-shield around the sides of the cooler has been provided. A passive Mo/Pb occulter, which modulates signals from within $\pm 5^\circ$ of the ecliptic plane at the spacecraft spin frequency, is used to identify and study solar flares, as well as emission from the galactic plane and center. Thus, in addition to transient event measurements, the instrument will allow the search for possible diffuse background lines and monitor the 511 keV positron annihilation radiation from the galactic center. In order to handle the typically large burst count rates, which can be in excess of 100 kHz, burst data are stored directly in an onboard 2.75 Mbit burst memory with an absolute timing accuracy of ± 1.5 ms after ground processing. The memory is capable of storing the entire spectral data set of all but the largest bursts. WIND is scheduled to be launched on a Delta II launch vehicle from Cape Canaveral on November 1, 1994. After injection into a phasing orbit, the spacecraft will execute a double lunar swing-by before being moved into a controlled 'halo' orbit about the $L1$ Lagrangian point ($\sim$ 250 R_e towards the Sun). This will provide a 5 light-second light travel time with which to triangulate gamma-ray burst sources with Earth-orbiting systems, such as those on-board the Gamma-Ray Observatory (GRO). The response of instrument to transient γ-ray events such as GRB's and solar flares will be presented as well as the expected response to steady state point sources and galactic center line emission.

[1] Department of Physics and Astronomy, University of Leicester, Leicester LEI 7 RH, U.K.
[2] CSSI, Columbia, MD 22046, U.S.A.
[3] Universities Space Research Association, NASA/GSFC, Greenbelt, MD 20771, U.S.A.
[4] GE Government Services, Lanham, MD 20706, U.S.A.
[5] EER Systems Corporation, Seabrook, MD 20706, U.S.A.

Space Science Reviews **71:** 273–296, 1995.

1. Introduction

The TGRS experiment is intended to perform high resolution spectroscopy of both transient and steady sources in the hard X-ray and gamma-ray region (0.01–10 MeV). There are a number of line-forming processes in this region that make it particularly interesting for spectroscopy. These include cyclotron, annihilation and nuclear processes. With the exception of a short-lived instrument in the ISEE-3 spacecraft, TGRS will be the first wide field-of-view, high resolution spectrometer to make space observations in the gamma-ray region. Sources to be studied include gamma-ray bursts, bright galactic transient sources, the galactic center region, the Crab Nebula and solar flares.

1.1. GAMMA-RAY BURSTS

Gamma-Ray Bursts (GRB's) were discovered accidentally by the Vela satellites two decades ago while verifying the compliance with (or monitoring) the nuclear test ban treaty (Klebesadel *et al.*, 1972). Since this time, they have been the subject of much experimental and theoretical study, but have remained one of the most enigmatic and intriguing of astrophysical phenomena. They are among the most violent and energetic processes known to exist in nature, characteristically emitting most of their luminosity at γ-ray wavelengths. Typically GRB's last from a fraction of a second to about a minute and are characterized by an impulsive rise and exponential decay. Substructure on tens of ms time scales can be discerned in most burst profiles. During the time of an outburst, the burst is usually the most luminous object in the γ-ray sky, being about a thousand times brighter than the ambient gamma-ray background. Although $\sim$ 300 such events have been reported each year by GRO, it has still not been possible to identify counterparts at other wavelengths or even find a convincing correlation with a specific class of astronomical objects despite many deep searches at specific GRB locations (see Hurley (1989a) for a review). Presently available GRB positions are consistent with an isotropic distribution in the sky. Since there is no consensus on possible counterparts, it is hardly surprising that the origins of γ-ray bursts are still unclear. Recent results from the BATSE investigation on GRO have extended the measurements of GRB locations to much weaker bursts and have remained consistent with isotropy. This, combined with the flat $\log N - \log S$ distribution for weak bursts, has led a number of investigators to postulate a cosmological origin for GRB's. If this hypothesis is correct, enormous energies ($\sim 10^{51}$ ergs) are required for GRB's.

Of particular significance, have been reports of 'line' features in GRB spectra which provide important clues to burst origins. Generally, they appear as broadened features at energies around 20–40 keV and 400 keV. Those near 30 keV are observed in about 20% of bursts and are interpreted as cyclotron absorption features produced in Tera–Gauss magnetic fields (Mazets *et al.*, 1981; Heuter *et al.*, 1982; Dennis *et al.*, 1981). The widths are uncertain, since most measurements have

been made with scintillation detectors and the features are clearly unresolved. Consequently, until the recent unambiguous GINGA detection of first and second harmonic features in the spectra of GB880205 (Murakami *et al.*, 1988), there had been considerable debate whether such features are absorption or emission lines or even whether they are authentic. Thus far, however, the BATSE experiment on GRO has failed to detect such features (Teegarden *et al.*, 1992).

The observed features near 400 keV are also controversial since few measurements have been made at the $> 2\sigma$ level. An examination of the available data suggests that such features occur in about 7% of detected bursts (Hurley, 1989b). They are generally broadened ($\Delta E > 200$ keV) and have been resolved by most experiments. They are interpreted as gravitationally redshifted positron annihilation radiation. The derived redshifts of $\sim$ 0.1–0.3, strongly suggest annihilation near a neutron star surface. Lastly, nuclear γ-ray lines might have been detected in the spectra of GB791119 (Teegarden and Cline, 1981). However, this interpretation is controversial because of marginal statistics and a clear confirmation must await future high resolution experiments such as the TGRS.

In view of the above problems, it is clear that measurements of burst spectra with high spectral resolution are essential. This would effectively eliminate the question of data compliance, leading to tighter constraints on possible emission models. The TGRS, with its excellent spectroscopic resolution, fine time resolution, large area and wide field-of-view (FOV) has been specifically designed to study all reported manifestations of bursts and is expected to contribute substantially to our understanding of GRB as well as transient phenomena in general.

1.2. SOLAR FLARES

Because the experimental design has been optimized towards transient phenomena, it follows that TGRS will be very sensitive to solar flares, since they are morphologically similar to GRB's. The advantages of performning high resolution spectroscopy on solar flares are numerous (for a review see Ramaty, 1986). For example, the solar flare, a direct manifestation of solar activity, allows us to study the coupling between the active corona and photosphere. Most importantly, such studies provide a direct channel with which to study particle acceleration and the impulsive release of energy in an astrophysical plasma. At present, several aspects of flares are poorly understood. For example, it is widely believed that the primary energy source for the flare is the solar magnetic field, possibly through magnetic reconnection. However, the dissipative process(es) by which this energy is turned into the observable flare are still unknown. Even at the most basic level, the question of charged particle acceleration and transport in flares is problematic. One of the best diagnostics of the above processes is the study of nuclear γ-ray lines. Such measurements provide direct evidence for the acceleration, confinement, transport and interactions of energetic electrons, protons and ions in flares. For example, the relative intensities of lines allow an unambiguous determination of the abundances

of the constituent matter within the flare region and useful pointers to the differential energy spectra of the interacting particles. The shape of such lines and any detectable shifts, provide information on the temperature and density of the ambient media in which they interact. Finally, such measurements also give information on the geometry of the flare region and more specifically, any anisotropies of the accelerated particles (Vestrand *et al.*, 1987).

1.3. GALACTIC SOURCES AND DIFFUSE EMISSION

An additional secondary objective will be to study the positron annihilation 511 keV line and the ^{26}Al 1809 keV line from the center of our Galaxy. To facilitate these studies, the signal will be modulated by a passive Pb/Mo occulter at the spin rate of the spacecraft (20 rpm). The primary goal is to monitor the time variability of the 511 keV line and three-photon positronium continuum from the galactic center region on time scales from $\sim$ 2 days to $>$ 1 year. Observations by balloon and satellite instruments over the past 20 years have indicated the presence of both a distributed positron source along the galactic plane which peaks at the center and one or more point sources (see Lingenfelter and Ramaty [1989] for a review). The emission from the point sources is assumed to arise from positron production near black holes, whereas the distributed component most likely originates from the decay of ejected nucleosynthetic positrons produced in cumulative novae and supernovae explosions. The lifetime of the positrons after they escape into the interstellar medium is of order 10^5 years which ensures that they will be well mixed with the interstellar medium before they decay, producing a diffuse source of very narrow line emission. Recently the Sigma instrument on the Granat spacecraft detected a time-variable feature near 511 keV from the Einstein source 1E1740.7–2942 near the galactic center (Paul *et al.*, 1991). The feature was seen during a single 13 hour observation, but not in observations 3 days earlier or 1 day later. TGRS will provide continuous high-resolution monitoring of this region. TGRS will also be sensitive to spectral structure in the cosmic diffuse γ-rays, which will dominate the detector background at low energies ($<$ 100 keV, see Figure 9). The statistical uncertainty in this measurement will be very small ($>$ 10^8 counts yr^{-1} in each 1 keV bin) allowing a sensitive search for lines in the spectrum.

2. The Instrument

The TGRS has been designed to meet all the above goals. Physically, it is similar to a smaller instrument flown on the Third International Sun–Earth Explorer (ISEE-3) mission (Teegarden and Cline, 1980), but with a substantial improvement in detector and cooler design. It has been chosen, under the Global Geospace Science (GGS) mission*, to fly on the WIND satellite due to be launched in November

* See, Science Plan for the Global Geospace Science Mission, International Solar-Terrestial Program, NASA, 1984.

1994. The KONUS investigation on WIND will also study GRB's. It consists of two large NaI detectors which will be mounted on the top and bottom of the spacecraft, aligned with the spin axis (defined to be the +z and −z axis). In addition to detecting bursts, the KONUS detector pair provides an independent confirmation of GRB events. The relative count rates recorded by the two detectors can be used to provide a burst source locus to within a few degrees relative to the spin axis.

The WIND laboratory is an ideal platform for TGRS from both a scientific and engineering point of view. Under the present plan, the spacecraft will spend a major fraction of its lifetime in a halo orbit about the $L1$ point, located on the Earth–Sun line some 250 earth radii inward toward the Sun. The spacecraft's spin axis will be oriented normal to the ecliptic. Thus sunlight will never strike the radiative cooler. Also, from a thermal point of view, the spacecraft is far enough away from the Earth that Earth albedo should not provide a significant heat input to the cooler. Because the $L1$ orbit is significantly outside the radiation belts, the detector will not be exposed to trapped radiation that typically degrades the performance of high resolution gamma-ray systems in low- Earth orbits. In fact the total dose (including 2 large solar flares) is calculated to be $\sim$ 8 krad over three years, as opposed to 18 krad expected in a typical 28° inclination, 500 km, low Earth orbit.

At the time of launch, there will be several other instruments in orbit that will be used to form an interplanetary timing network. Perhaps the most notable, is the Burst and Transient Spectroscopy Experiment (BATSE) on-board the Gamma-Ray Observatory, launched in April 1991. BATSE has excellent sensitivity but only modest spectroscopic resolution. In contrast, TGRS has over 20 times BATSE's spectral resolution. The two instruments will therefore, complement each other. TGRS will be able to analyze spectral features in detail which BATSE cannot resolve, whereas BATSE will be able to detect much weaker features and study time variations of the more intense features in great detail. Finally, since during the latter half of the mission, WIND will be stationed at the Lagrangian point it will afford a short baseline which to triangulate burst locations (almost 6 light seconds). When coupled with other long baseline investigations sensitive to GRB's such as ULYSSES, the Mars Observer Mission and The Soviet Mars '94 Mission, timing studies will lead to the possibility of arc-min source fields for the brighter bursts.

2.1. MECHANICAL

An exploded view of the instrument and its location on the spacecraft is shown in Figure 1. It has four principal components namely, a detector/cooler assembly, preamplifier, Analog Processing Unit (APU), and a Digital Processing Unit (DPU). Each of these subsystems are described in detail in the following sections. The mechanical design criteria were;

– the ability of the detector module to survive 100 g's axial loading to withstand the rigors of a Delta II launch,

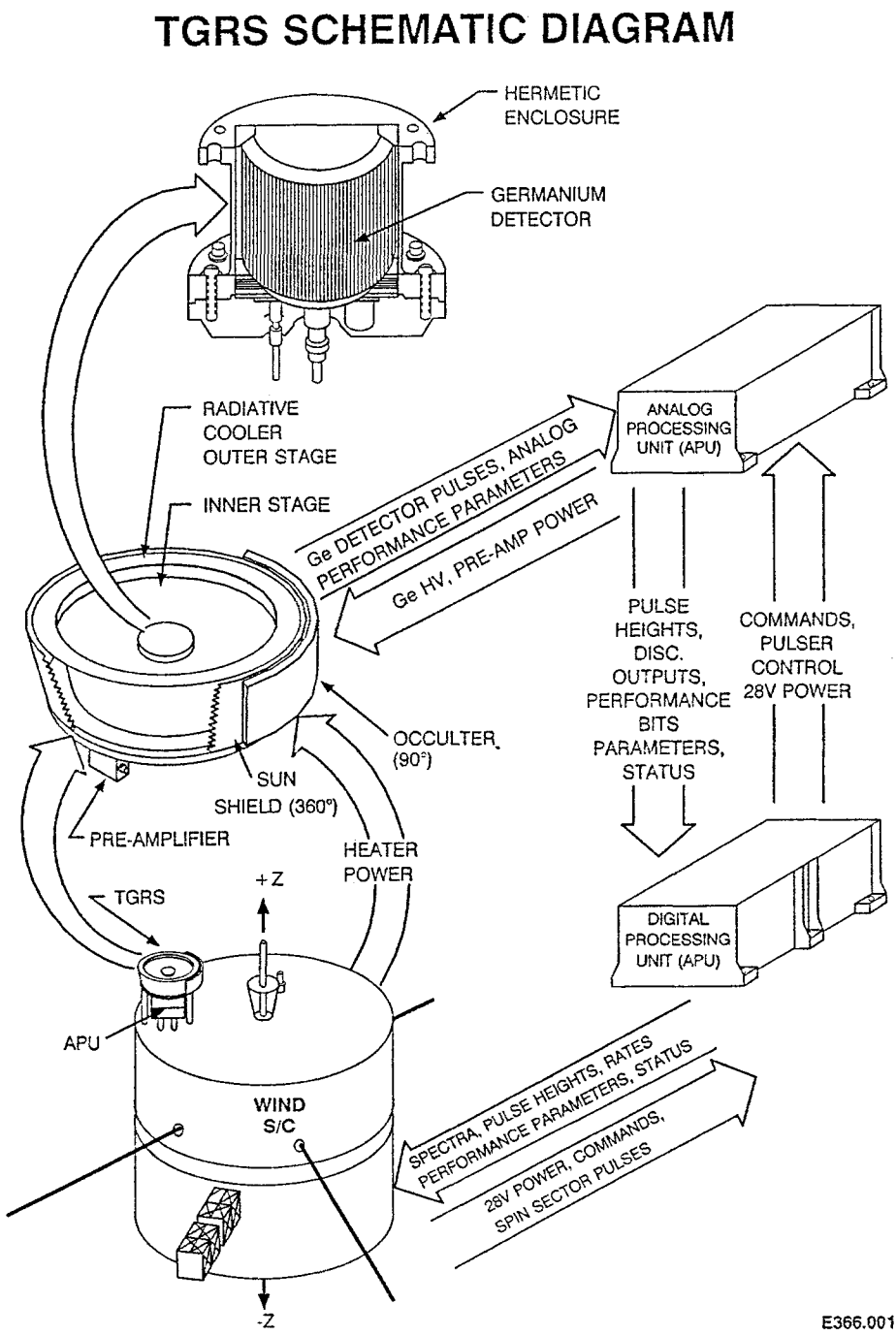

Fig. 1. An exploded view of the instrument showing the primary TGRS components in relation to the WIND laboratory and the signal and data flow at the systems level.

– the use of low z material throughout the cooler/detector assembly to ensure that the material surrounding the detector is transparent to burst radiation down to X-ray wavelengths ($\sim$ 25 keV) and,

– to maintain a clean environment for the Ge detector. For example, minimizing the use of plastics such as Teflon and Vespel in the detector module assembly which are known to desorb over long periods of time.

The central detector is a large n-type Ge crystal, cooled to cryogenic temperatures by a passive radiative cooler. Physically, the detector/cooler assembly is mounted on a cylindrical tower secured to the upper equipment deck. The tower rises far enough above the top of the spacecraft (the spin axis) to ensure that the nearly hemispherical TGRS FOV is clear of most projections and obstructions originating from the spacecraft and the other instruments. This is particularly important in radiatively cooled systems, since such obstructions will be at significantly higher temperatures than deep space ($\sim$ 3 K). Unfortunately, the z-axis antenna does impinge on the cooler FOV. This device is part of the WAVES investigation and when fully deployed is of length 6.5 m and diameter 2.9 cm. The surface finish has been specially chosen to reduce the amount of reflected sunlight into the cooler. Additionally, the antenna 'seams' are oriented so that, they are out of the FOV. Under the worst conditions, a detailed thermal model has shown that the net effect is to raise the cooler temperature by a few degrees.

Active shielding techniques have not been employed, since for most bursts it is the burst itself that constitutes the dominant source of detector background when attempting to discern γ-ray lines or structure in the spectrum. Therefore, any modest gain in signal to noise ratio would be more than outweighed by the loss of FOV and the increase in weight, power and complexity. However, a 30 mil thickness Be/Cu alloy passive-Sun-shield has been included around the sides of the cooler to ensure that the instrument is not continually triggered by soft solar events, such as the frequent 'micro-flare' events reported by Lin *et al.* (1985). The shield is calculated to attenuate solar X-rays by a factor of 1000 at 20 keV falling to $\sim$ 3 at 40 keV.

Surrounding a quarter of the outer diameter of the cooler is a 13.5 mm thick passive Mo/Pb strip of thicknesses 1.5 and 12 mm, respectively, which acts as an occulter for sources in the ecliptic plane. The molybdenum acts as a passive shield for fluorescent photons produced in the lead. The axis of symmetry of the cooler is co-aligned with the spin axis of the spacecraft, which is perpendicular to the ecliptic (within 0.5°). During normal operation, the occulter modulates signals originating from within $\pm 5°$ of the plane of the ecliptic at the spin frequency of the spacecraft. This signal will be used primarily to study the galactic plane emission (including the center) which lies $\sim 4°$ above the normal to the spin axis. The occulted signal is modulated over $\pi/2$ radians and is reconstructed modulo fashion *post apriori*. Such information, when combined with the spacecraft Sun sensor data, is also used to generate a solar event flag. This signal is used to tag solar events for later analysis and is made available to the KONUS investigation.

TABLE I
TGRS characteristics

Detector	High purity n-type germanium crystal in the reverse electrode configuration
Dimensions	6.7 diameter × 6.1 cm length; volume 215 cm^3
Energy range	25 keV to 8.2 MeV
Energy resolution	~ 3 keV @ 1 MeV
Photopeak efficiency	43% @ 511 keV
	16% @ 1809 keV
Field-of-view	170° FWFM geometric
Sensivitity	better than 10^{-7} ergs cm^{-2} for 60 s burst duration
Subsystems	Detector
	Cooler
	Analog Processing Unit (APU)
	Digital Processing Unit (DPU)
Occulter	Modulation factor in the ecliptic plane=25%, attenuation ~ 10 @ 511 keV
Cryogenics	Two stage passive cooler of radiating area ~ 1600 cm^2
	inner stage temperature 85 K; outer stage temperature 164 K
	detector/cooler assembly weight 6.1 kg
	dimensions 46 cm dia × 17 cm thick
Temporal resolution	62 μs intrinsic; ±1.5 ms after ground processing
Memory size	2.75 million bits
Bit rate	376 bit s^{-1}
Total weight	18.23 kg
Total power	6.95 W quiescent
	26 W heater power (low duty cycle)

2.1.1. *The Germanium Detector*

The instrument was designed around a 215 cm^3 high purity Ge crystal manufactured to order and fabricated into a detector by the semiconductor spectrometer group at the Lawrence Berkeley Laboratory (LBL). Its specifications are listed in Table I. The detector assembly is unusual, in that it has been designed as an integral hermetically sealed unit that can be thermally cycled from room temperature (22 °C) to liquid nitrogen temperature (−196 °C) without degradation. The detector is an n-type closed-end coaxial of diameter 6.7 cm and length 6.1 cm in the reverse electrode configuration.

Figure 2 shows a cross-sectional view of the completed detector module assembly. The crystal has an outside bevel at both ends which is used to clamp it within the detector enclosure. A 2 mil gold foil, placed inside the lower bevel makes mechanical contact with the crystal and serves as the electrical ground return. The inner HV connection to the Li diffused n^+ contact is made with a coaxial compression contact spring mounted on a high voltage feed-through. Below the bottom face of the crystal is the enclosure cover which serves as the lower seal of the

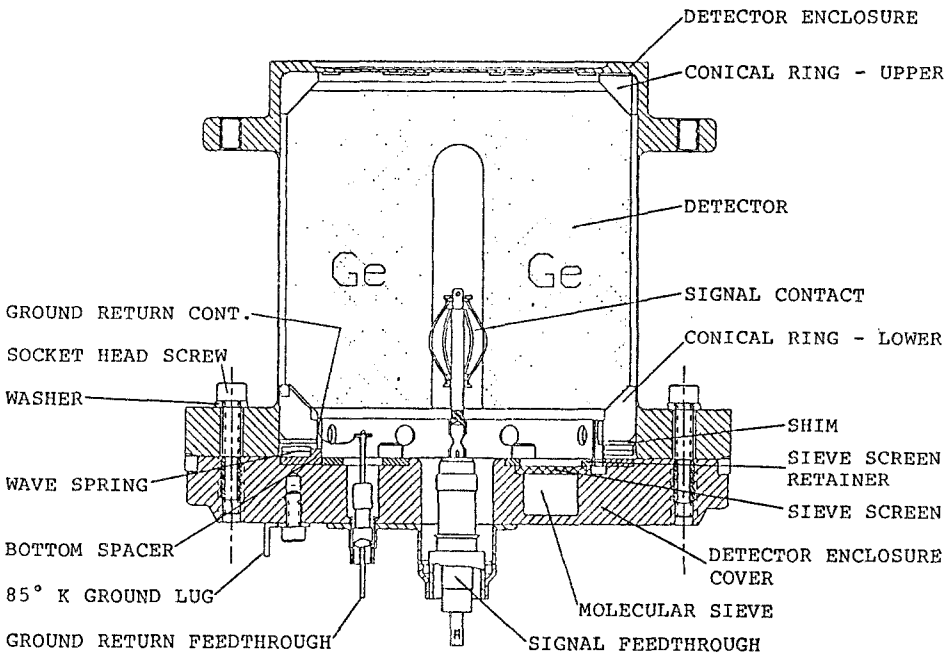

Fig. 2. A cross-sectional view through the Ge detector module.

detector assembly and contains 3 pockets. Two pockets contain approximately 1 cc each of Union Carbide SA molecular sieve. The third pocket contains $\sim$ 0.5 cc of paladium oxide getter material to trap hydrogen. The holes are covered by 40 μ screens which are small enough to prevent sieve material passing into the detector module, but large enough to allow the sieve material to pump the volume. A fourth pocket, located on the outer surface of the detector enclosure, contains a γ-ray calibration reference consisting of $\sim$ 1 cc of potassium sulphate. This emits monoenergetic γ-rays of energy 1460 keV which are used to monitor the linearity and stability of the analog signal chain. This amount of compound is calculated to give an induced count rate at the detector of 4 cts min^{-1}. The detector enclosure is made entirely from aluminum. The seal between the upper enclosure and the lower cover is achieved using an indium O-ring. A wave spring provides the preloading force to clamp the crystal within the enclosure. The module is assembled and sealed in a custom-built bell jar which provides for bake out, UV flood and hermetically sealing the crystal within the enclosure.

2.1.2. *The Radiative Cooler*

Since an on-board annealing capability is not being built into TGRS, the cooler was designed to maintain the temperature of the detector below 85 K throughout the mission lifetime. This ensures that the effects of radiation damage on the detector performance are minimized. A cross-section of the cooler is shown in Figure 3.

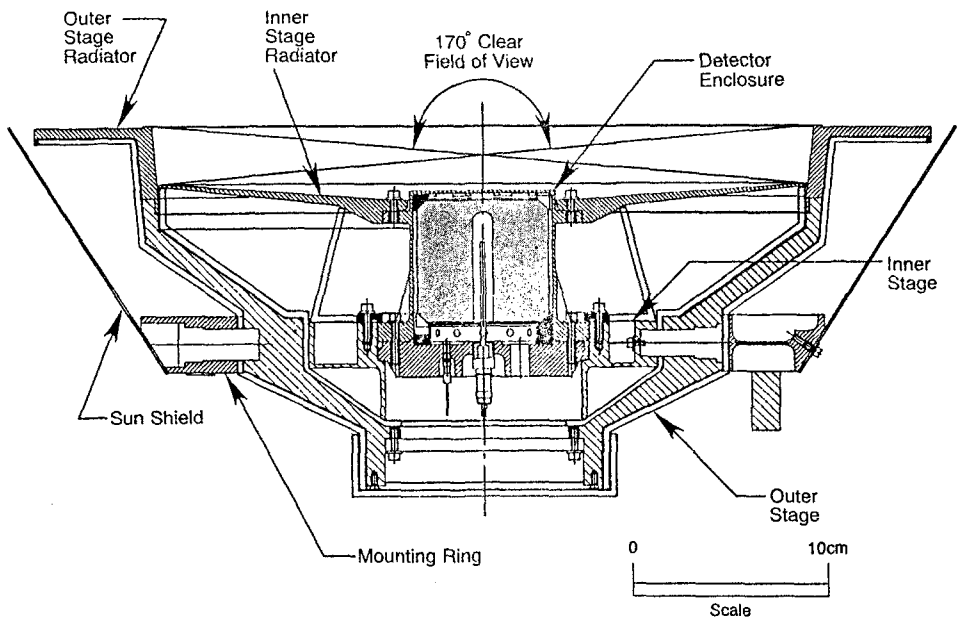

Fig. 3. A cross sectional view of the radiative cooler. A grid of fine Be/Cu wires that covers the outer stage aperture is not shown for clarity.

It is functionally similar to a design flown on the ISEE-3 mission (Teegarden and Cline, 1980) and has two stages; an outer stage and an inner stage coupled to each other and the spacecraft by three low-conduction supports of small cross-section. In essence, the inner and outer stages reject heat by radiation to space. The outer stage is designed to operate at an intermediate temperature (164 K) and thereby provide a thermal buffer between the detector and the spacecraft. The mechanical interface between the outer-stage and the TGRS tower is a support ring which is maintained near room temperature. As the outer-stage cools, it contracts slightly. The support points are designed such that this contraction breaks the thermal path between the support ring and the outer stage, thereby thermally isolating the cooler. Similar support points for the inner-stage break the thermal path between the inner and outer stages. Both sets of support points are offset by 60° to each other to increase the thermal path length (and consequently minimize heat flow) from the tower to the inner stage through the supports.

The cooler has a conical shape which defines a geometric FOV of 170° full angle. Obviously, for the cooler to operate correctly, the aperture must be free from heat sources such as the Earth, Sun or any significant portion of the spacecraft. The cooler is constructed of Be and Mg to minimize weight and X-ray attenuation. The radiation surfaces of the inner and outer stages are fabricated entirely from Be. To prevent stray fields generated by spacecraft charging from interfering with the on-board electric field experiments, the forward cooler aperture is screened by a grid

of fine 2 mil Be/Cu wires. A complete thermal analysis has shown that the inner and outer stages will reach equilibrium temperatures of 85 and 164 K, respectively. Immediately after achieving orbit, an internal 26 W heater mounted to the outside of the outer stage, will raise the inner stage temperature to $\sim$ 20 °C to prevent outgassing spacecraft contaminants from condensing on the radiative surfaces. Experience with the Air Force Defense Meteorological Satellites has shown that such contaminants degrade cooler performance. The cooler will be baked out for 7 days. Finally, the effects of contamination from the hydrazine thruster plumes have been evaluated and shown to be negligible and in fact, slightly beneficial, since such deposits tend to raise the overall emissivity of the cooler.

2.2. ELECTRICAL

The detector electronics consist of four sub-components. These are: the 170 K card (located directly under the detector enclosure); the detector preamp (which is housed in a metal box attached to the underside of the cooler mounting ring), the Analog Processing Unit (APU) which is mounted inside the TGRS tower, 6 inches below the cooler, and the Digital Processing Unit (DPU) which is located below the spacecraft tower on the upper equipment deck. A system-level schematic of the signal and data flow is shown in Figure 1.

2.2.1. *The Analog Electronics*

A functional block diagram of the analog electronics is shown in Figure 4. The output charge pulse of the Ge detector is AC coupled to the front end of a low power preamplifier (160 mW including the FET). The front-end components, i.e., the input FET, preamplifier feedback components, leakage current monitor and detector high voltage biasing components, are mounted on the 170 K card. The individual components are captured in Teflon to protect them during the rigors of launch. The temperature of the card is maintained at the outer stage cooler temperature (i.e., 170 K), ensuring that the input FET operates in the low-noise region of its characteristic.

After pre-amplification, the signal is passed to the shaping amplifier which contains a slow shaper, fast shaper, fast discriminator, pile up rejection logic and pulser circuitry. The slow shaper uses a four-pole pseudo-Gaussian shaper with a second differentiator (bipolar shaping). The peaking time is commandable from either 8 μs or 2 μs. Under normal operation, it will be set to 8 μs to ensure good energy resolution. However, if the detector begins suffering significant spectral degradation because the performance of the cooler deteriorates, it will be switched by command to 2 μs. A Test Pulse Generator (TPG), or pulser, has been incorporated into the APU to verify the operation of the analog chain, even when the detector is at room temperature. Upon receipt of a commandable pulse from the DPU, the circuitry disconnects the preamplifier and applies a periodic signal (equivalent to 100 keV) to the input of the shaping amplifier.

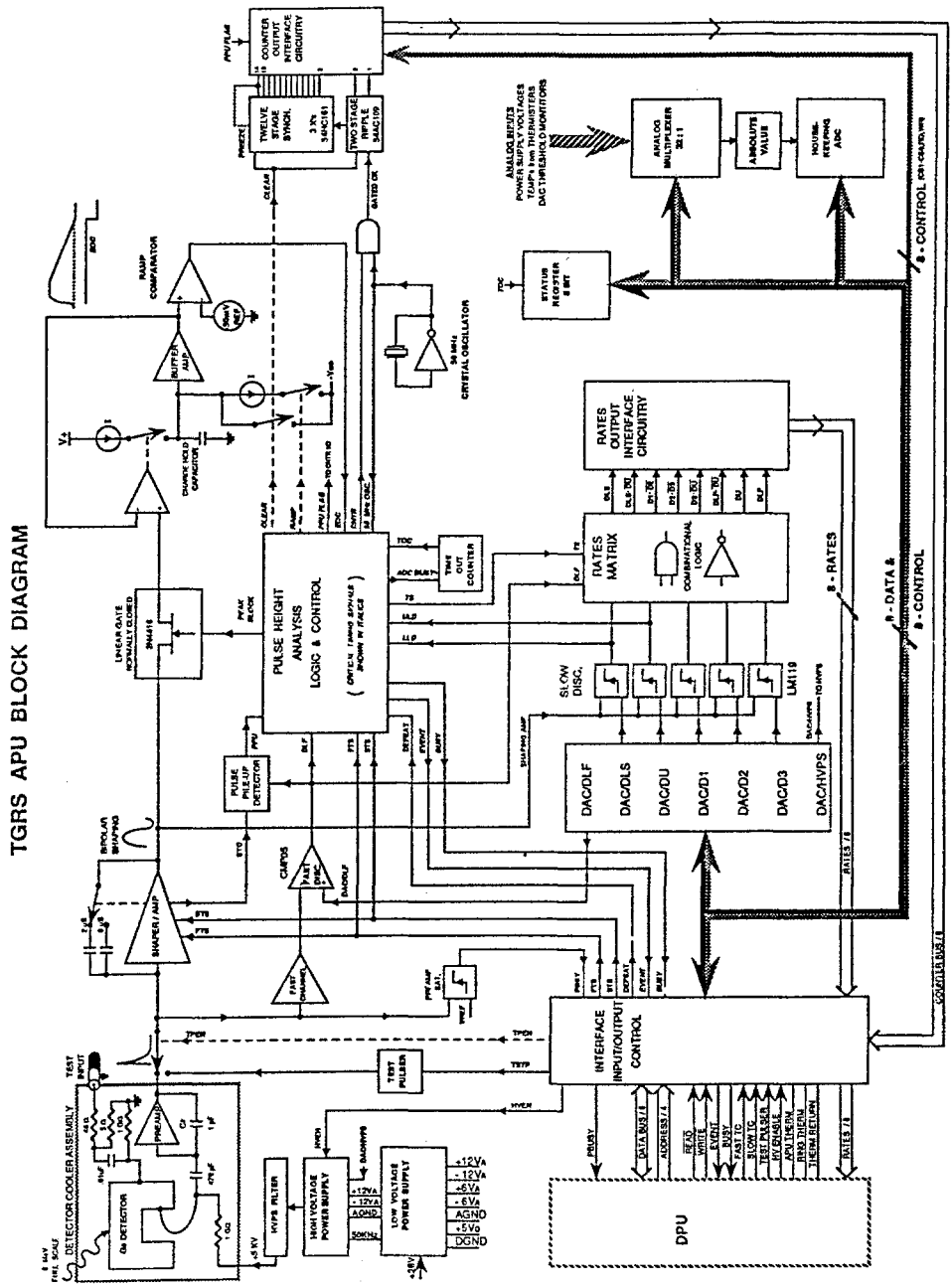

Fig. 4. A functional block diagram of the analog processing electronics.

The output of the amplifier is fed to a 13-bit Wilkinson ADC operating at a clock frequency of 50 MHz. The analysis of an event is dependent on certain selectable criteria, namely, that the signal is greater than the lower discriminator threshold, less than the upper discriminator threshold and the pulse pile-up flag is not set. The upper and lower level discriminators are nominally set at 8.1 MeV and 15 keV, respectively. The overall differential and integral non-linearity of the analog chain have been measured to be $<1\%$ and 0.05%, respectively over the top 99% of range. The high voltage for the Ge detector is derived from a commandable 0 to 5 KV bias supply controlled by an 8-bit DAC.

2.2.2. *The Digital Electronics*

The digital electronics are shown schematically in Figure 5. The primary functions are to

(a) acquire and process pulse height data from the APU, (b) accumulate background and burst spectra and various count rates, (c) format and read out data into the spacecraft telemetry stream, (d) control the basic mode of operation of the instrument; i.e., waiting, burst or dump, (e) decode and execute instrument commands.

The instrument has three basic modes of operation. These are the 'waiting mode' in which the instrument waits for a burst to occur; the burst mode, in which the instrument receives and processes burst data; and the dump mode in which the instrument releases burst data to the spacecraft telemetry. At the expected burst rate of approximately two events per week (not including solar and spurious triggers), the experiment will spend a large fraction of its time in the waiting mode. In this mode, the instrument continually scans for the signature of a burst. During this time, the DPU records pre-burst data using $\sim$ 10% of the memory. The type of data stored is given in Table II along with the approximate memory allocations during the waiting mode. The data include histograms of events below ADC channel 200; event-by-event storage of events above channel 200; rate profiles, and 128 spin modulated histograms, each with 64 energy channels corresponding to a 2.81° rotation of the spacecraft. Additionally, the flight program forms 1024 and 8192 channel histograms of germanium spectral data integrated over 3 and 24 mins, respectively; these times are commandable. These data are used to determine the background level during a burst or solar flare and fulfill the secondary science objectives. The accumulations are carried out in double-buffered memory in order to reduce dead time. The 1024 and 8192 channel histograms, along with housekeeping functions, are read out to the spacecraft telemetry stream.

In the burst mode, data are stored directly in a 2.75 Mbit burst memory, since the expected data rate during a burst will be far higher than the nominal TGRS telemetry bit-rate of 376 bits s^{-1}. Events above channel 200 are digitized event-by-event, time-tagged to 62.5 μs and stored directly. Because burst spectra can be very soft and the incident burst fluence can be very high, low-energy events are pre-binned into 200 channel (1 channel $\approx$ 1 keV) histograms before storage in order not to

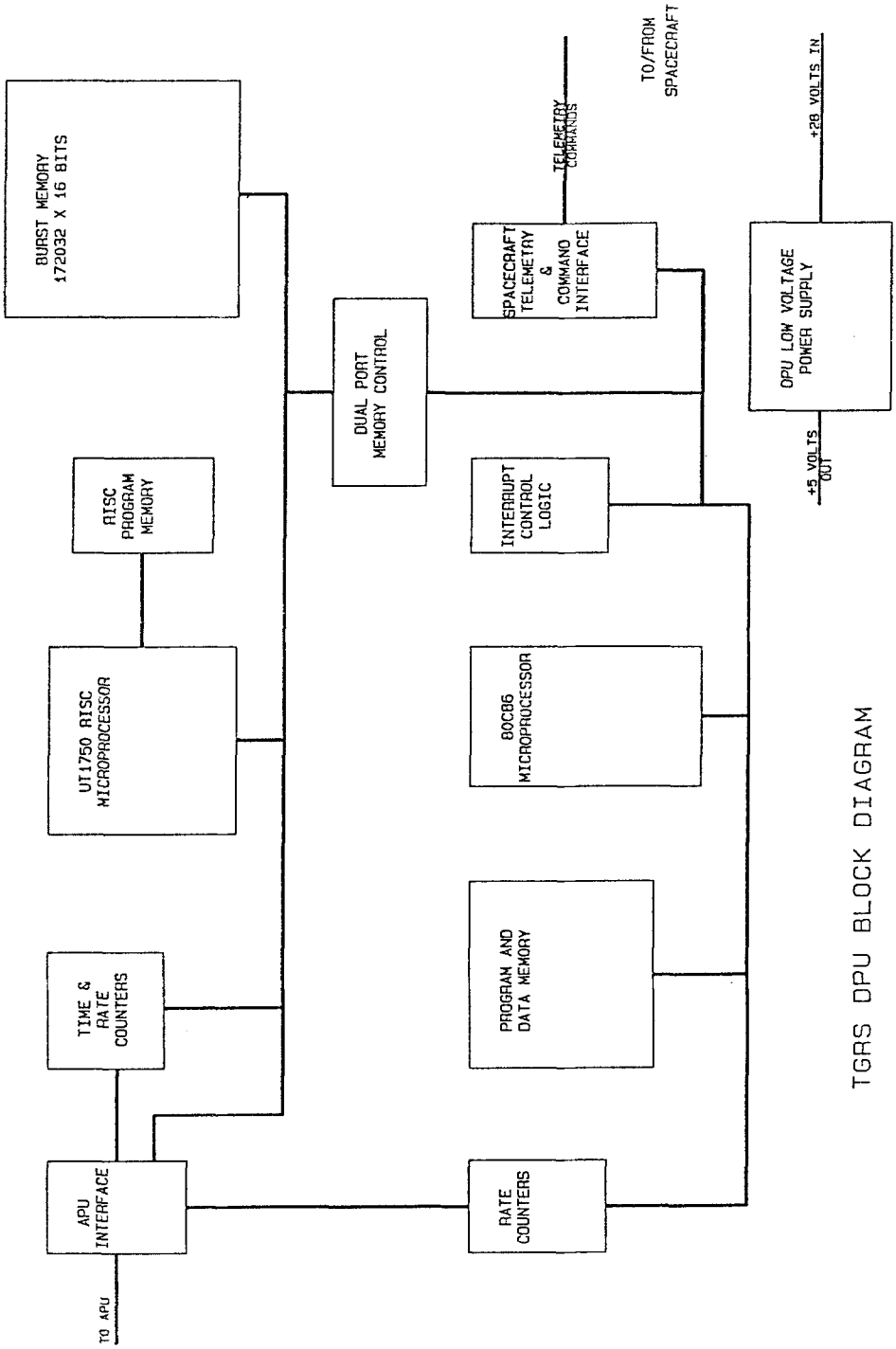

Fig. 6. A functional block diagram of the digital processing electronics.

TABLE II

TGRS waiting mode memory allocation[a]

Data type	Memory allocation (16-bit words)
Event-by-event above ADC ch 200	110 K
200 ch histograms	45 K
1024 ch spectra	2 K
8192 ch spectra	16 K
Sectored windows 64 ch's, 4 energy ranges	50 K
11 rates	12 K

[a] In the burst mode, the event-by-event data occupies an additional 70 K, 16-bit words (the sectored windows, 1024 and 8192 ch spectra are not accumulated in this mode).

incur significant dead time. After ground processing the absolute timing accuracy is estimated to be ± 1.5 ms. The detection of a burst is accomplished by two independent trigger algorithms which continually sample the detector count rate and initiate a trigger if, and only if, the count rate exceeds a predetermined level, set by ground command. The trigger threshold is commandable and is normally set for an increase of 9 standard deviations above the expected quiescent background rate of $\sim$ 500 cts s^{-1}. At this level, TGRS is expected to detect over 100 bursts yr^{-1} above a size threshold of a few times 10^{-7} ergs cm^{-2}. When a trigger occurs, data are stored directly in the burst memory. During this time, a limited amount of data (about 20% of normal) is telemetered to the ground. After 20 min have passed, or the memory is full, the instrument is switched to the dump mode, after which the burst memory is read out. The telemetry stream consists of about 70% event-by-event germanium pulse height data above channel 200 (digitized by the on-board 12-bit ADC), supported by infrequent readouts of the housekeeping data. Count rate and dead time information is stored as well. Since burst spectra are generally very soft, the lower channel pulse height data (channels 1–200) are read out as 500 count histograms, to reduce the demand on onboard memory. The burst memory readout time is estimated to take <2 hours. At the end of this time, the flight program returns the instrument to the waiting mode and resumes the search for burst events.

The DPU architecture is based on two microprocessors. A Harris 80C86, running at 5 MHz, is used to perform the command and data handling functions, control the DPU mode and burst detection, collect the DPU and APU housekeeping and status, and accumulate the rates and live-times. A United Technologies UT1750AR Reduced Instruction Set Computer running at 12 MHz does the actual event handling, essentially acting as an 'event engine' for the DPU. It reads the PHA events from the APU, updates the appropriate histograms and stores events directly in burst memory according to the current processing mode. In addition, the 1750 services the time-to-spill counters.

2.3. FLIGHT SOFTWARE

The UT1750AR microprocessor is configured to run in its native RISC mode, and is capable of executing 6 million RISC instructions per second. Its primary task is to process pulse height events as they are presented by the APU. The software consists of a background routine and several prioritized interrupt service routines. When a burst is detected, it can process and store incoming events at an average of 10 μs per event, until the memory is full. The 80C86 microprocessor handles the command and telemetry functions, the analog and digital housekeeping, and the hardware rate counters. It periodically extracts the processed events (histograms, rate samples, and raw event samples) from the dual-ported 1750 operand memory and formats them for telemetry. It also analyzes the event rate data for a burst signature and triggers the 1750 burst storage for count rates exceeding a predefined level. When the burst storage is complete, it extracts and formats the burst data for telemetry.

3. TGRS Data Analysis

The bulk of the analysis, such as spectral unfolding, etc., will be carried out on a workstation based system, configured from one MicroVax 3100 model 10e (4 + 16 MB RAM, and an additional 1 GB hard disk), and one VaxStation 3100 model 76 (12 MB RAM) supported by a 19″ high resolution monitor and DEC windows. Archived data are imported using a second optical disk drive connected to the DEC SCSI interface.

The TGRS data analysis system will be based on data analysis software originally developed for the BATSE investigation on the Gamma-Ray Observatory (GRO). It will generate time histories and count spectra (source, background, and background subtracted source). It further performs spectral model fits, finds the errors associated with the fitted model parameters, produces photon spectra, calculates fluences, etc., and finally organizes the results in a 'processed data' data base which will be centered on the INGRES®) relational data base system. Material for publication (e.g., figures, various fitted and calculated parameters) can readily be extracted from this data base. Additionally, a visual display package, based on the interactive data language IDL®, is being developed at Marshall Space Flight Center which may be used as a stand-alone package for certain data analysis and display tasks. Coupled with custom user programs and the considerable case tools available with VMS, the software will provide a powerful data analysis system allowing the acquisition of TGRS data by INGRES by type (e.g., geomagnetic coordinates, L and B, time or anything else), manipulation and visualization by IDL, and final processing from experimenters units to scientific units by user supplied programs.

4. Instrumental Performance

4.1. INSTRUMENT BACKGROUND

The TGRS background has been predicted using semi-empirical and Monte-Carlo calculations and is shown in Figure 6. The error in the total is expected to be no more than $\sim$ 50%. From the figure it can be seen that the background spectrum is comprised of three principal components. At low energies, the cosmic diffuse γ-rays dominate. At intermediate energies, from say 0.1 to 2 MeV, local production within the spacecraft itself becomes the largest source of noise. This component arises from the intra-nuclear reactions of cosmic-rays with the material of the instrument and spacecraft resulting in fragmentation, nucleon cascade and evaporation. The reaction products, both charged particles and neutrals, may then interact directly in the detector or interact in the spacecraft producing secondaries which in turn interact in the detector. This component was scaled from ISEE-3 measurements. Above a few MeV, cosmic-rays dominate the spectrum forming a flat continuum to 10 MeV. This component was also estimated from ISEE-3 measurements.

4.2. DETECTION EFFICIENCY

The detector efficiency has been evaluated using the EGS4 Monte-Carlo photon-electron transport code. It considers all primary and secondary interaction processes including photoelectric, Compton, pair and bremsstrahlung as well as the ionization energy losses of seeondary electrons. Particles are transported until they escape from the instrument or lose all their energy. The results are shown in Figures 7 and 8. In Figure 7 the calculated TGRS photopeak effective area for normal incidence is shown as a function of energy. Also, shown are the total effective area and the effective areas for single and double escape interactions. (These are interactions where the primary photon undergoes pair production, the positron annihilates in the detector, and one or both of the 511 keV annihilation photons escape from the detector.) In Figure 8 the calculated TGRS low-energy photopeak effective area is displayed as a function of incidence angle for different energies. It can be seen that the relative responses are relatively insensitive functions of angle to $\sim$ 70°. This means that the incident source spectrum may be unfolded relatively easily, given a crude input source direction which can be supplied by the KONUS investigation. By comparing the count rates in the two KONUS detectors, it should be possible to provide a burst location in the zenith plane (i.e., with reference to the z-axis) to within + 5°. Given the azimuthally symmetric, relatively flat response of TGRS, this should lead to errors in the unfolded burst spectra of no worse than 15%. Thus, unfolded spectra can be produced in near real time. For incident angles >110° the detector becomes occulted by the spacecraft itself. We estimate that for angles between $\sim$ 110° and 225° the spacecraft represents an equivalent thickness of 12 cm of aluminum (33 g cm^{-2}).

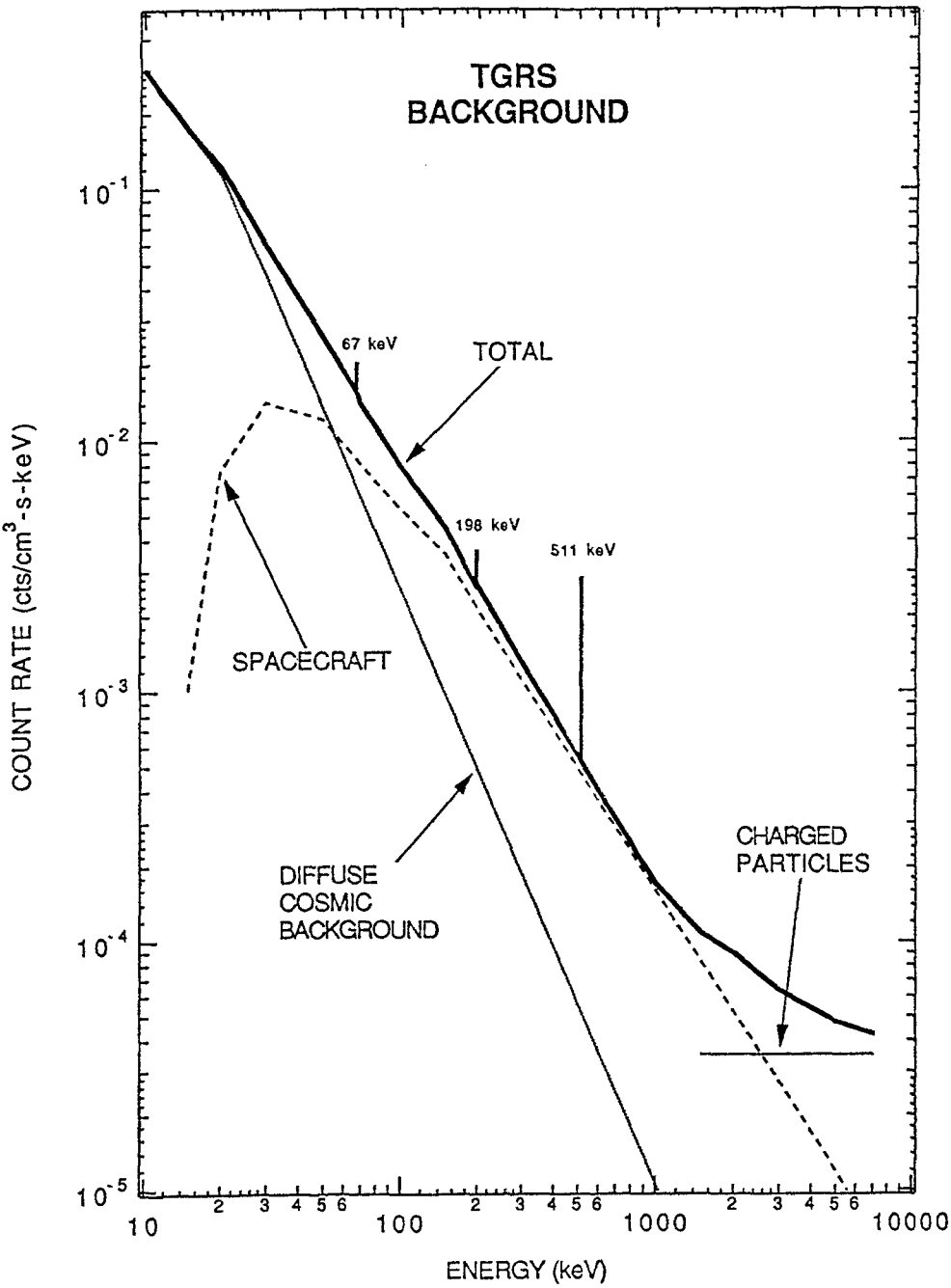

Fig. 6. The predicted TGRS background spectrum. The various contributions are described in the text.

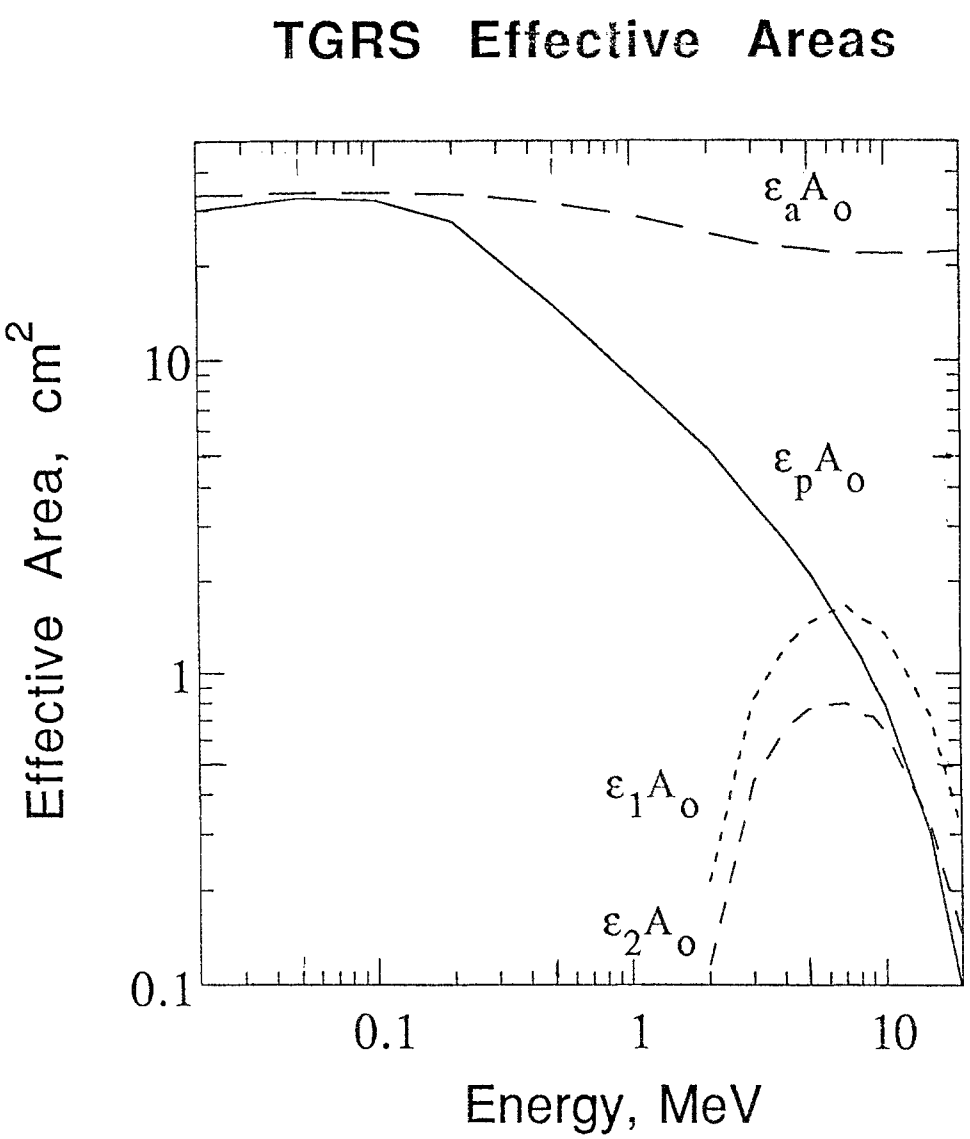

Fig. 7. TGRS effective area vs energy. ϵ_a = total efficiency, ϵ_p = photopeak efficiency, ϵ_1 = single escape efficiency, ϵ_2 = double escape efficiency.

4.3. RESPONSE TO GAMMA-RAY BURSTS AND SOLAR FLARES

The response of the instrument to γ-ray bursts and solar flares has been evaluated. For example, a generic burst spectrum of size 10^{-5} erg cm^{-2}, integrated over 1 s, will produce an energy loss spectrum which is comparable to the detector background above $\sim$ 1 MeV. The calculated spectrum is shown in Figure 9. For comparison, we also show the predicted background. For this burst the signal

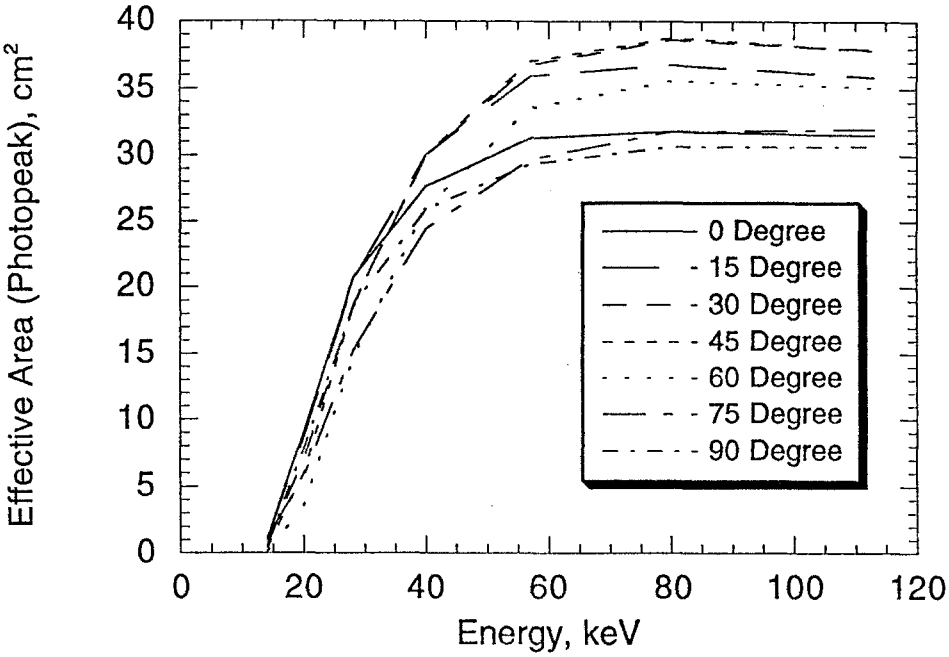

Fig. 8. The calculated TGRS low-energy photopeak effective area as a function of energy for different incidence angles.

would have been detected at the $\sim 30\sigma$ level above threshold. In Figure 10 we show the instrumental sensitivity to spectral features for a variety of burst fluences. To derive meaningful figures for absorption features, the sensitivities are plotted as equivalent widths divided by the center energy. For comparison, we also show the derived equivalent widths for reported features, plotted on the same graph. It can be seen that for burst sizes above 10^{-5} erg cm^{-2}, TGRS would detect all the previously reported line features.

The effectiveness of the Sun shield has been evaluated for both solar flares and microflares. Averaging the four largest microflares observed by Lin *et al.* (1984), we find that the Sun shield will attenuate the incident spectrum by a factor of 103 at 20 keV, falling to 20 at 50 keV. Likewise, for the intense 1980 June 4 flare, we find that the incident $E^{-3.9}$ spectrum at X-ray energies is modified significantly by the shield, reducing the integral flux in the energy band 20 to 100 keV from $\sim$ 14 000 counts s^{-1} to $\sim$ 800 counts s^{-1}. In Figure 11 we show the TGRS response to the nuclear line-rich April 1981 flare which lasted 1700 s. The upper curve shows the response in an equivalently sized NaI detector to this flare, which clearly underscores the need for high resolution measurements.

Finally, it is interesting to note that TGRS will also be sensitive to solar neutrons. For example, using the 691 keV line (which arises from the de-excitation of the O^+ first excited state of ^{72}Ge) it is possible to get a direct measure of the integral neutron

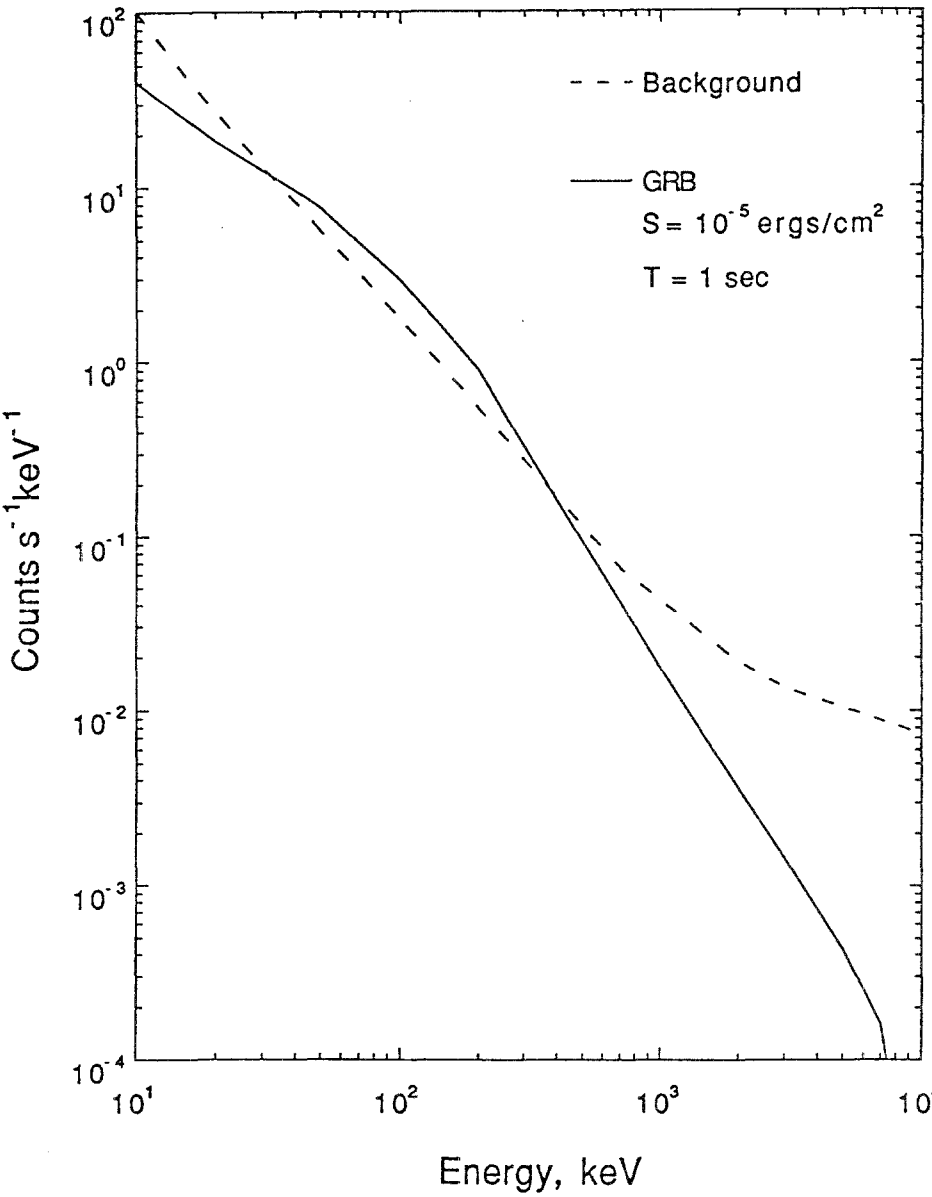

Fig. 9. Predicted response to a generic burst spectra of size 10^{-5} erg cm^{-2}, integrated over 1 s. For comparison we also show the estimated background spectrum.

fluence above threshold, since the cross section is independent of energy. Thus, it should be possible to separate the prompt and delayed solar emissions, something that has not been possible with NaI based instruments, such as the SMM/GRS. Additionally, measurements of the time history of the 2.2 MeV neutron capture line yield information on the low energy neutron spectrum and thermalization times

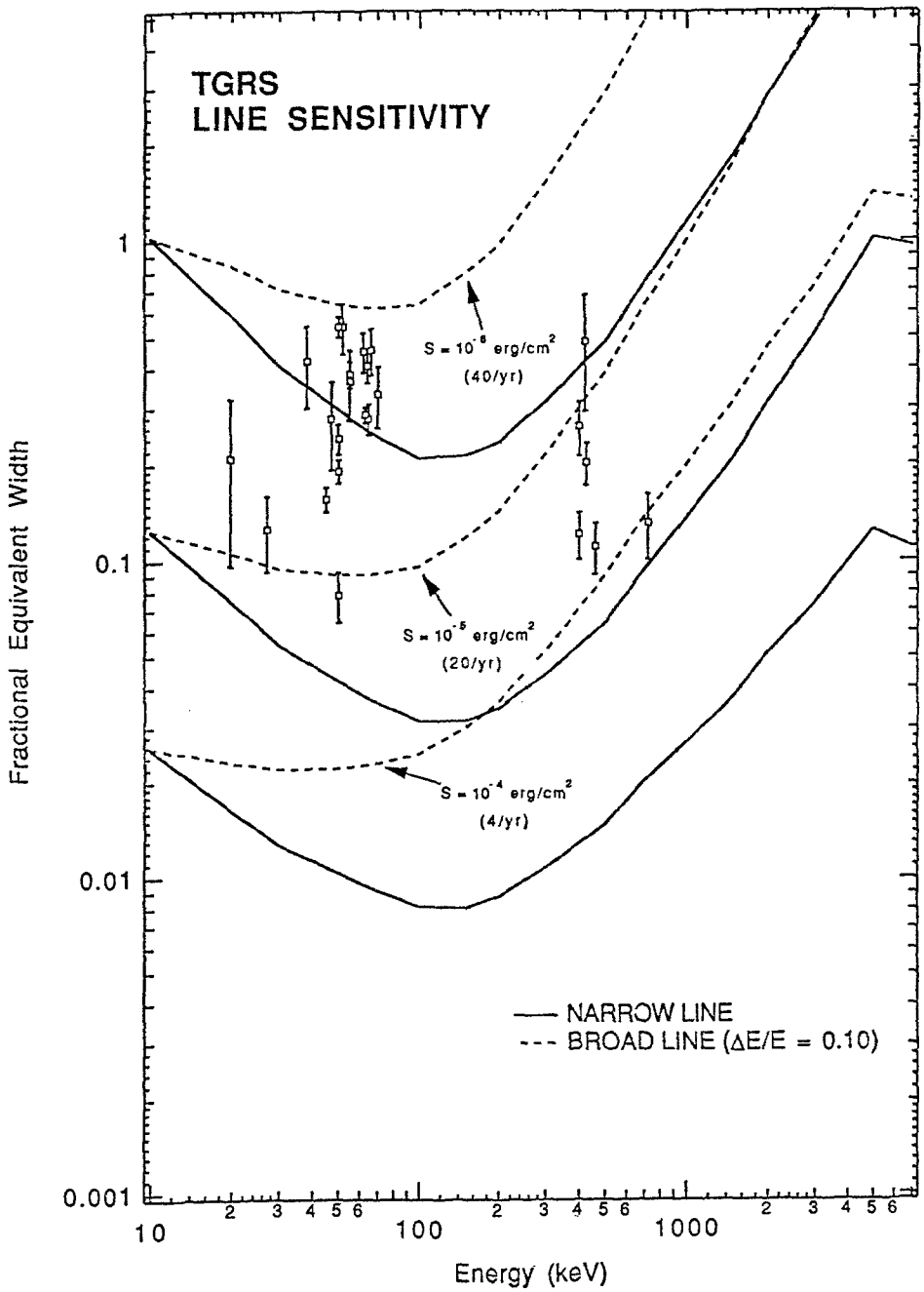

Fig. 10. The instrumental sensitivity to spectral features for a variety of burst fluences. In order to derive meaningful figures for absorption features, the sensitivities are plotted in the form of equivalent widths divided by the line energy. For comparison, we also show the derived equivalent widths for reported features.

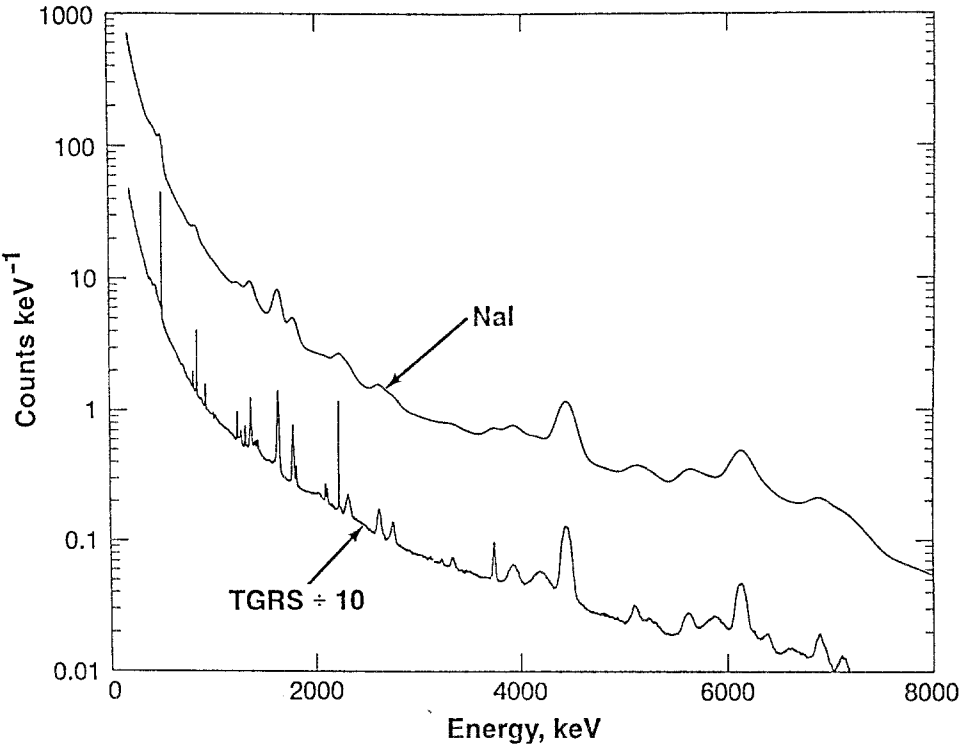

Fig. 11. The TGRS response to the nuclear line rich April 1981 flare. The upper curve shows the response of a similar sized NaI detector to this flare which clearly underscores the need for high resolution measurements.

in the photosphere. A preliminary estimate suggests that we can detect the neutron flux from the 1980 June 3 flare at the 10σ level. Lastly, TGRS will also be very sensitive to solar neutron decay protons if tied to a favorable field line (Evenson, 1988). An exact determination of the sensitivity is difficult since it is dependent on the field geometry as well as the proton storage time in the interplanetary magnetic field.

4.4. Spectrometer Response to Point Sources

The response of the instrument to steady point sources has been estimated. It was assumed the signal will be derived by comparing the occulted/unocculted signals summed modulo fashion. The occulter attenuates the spectrum by a factor of 100 below 200 keV and a factor of 3 at 1 MeV. For the reported line features at 511 and 1809 keV from the galactic center, the signal will be modulated by a factor of $\sim$ 10 and 1.8, respectively. Assuming line fluxes of 1×10^{-3} photons cm^{-2} s^{-1} and 4×10^{4} photons cm^{-2} s^{-1} rad^{-1}, respectively, it is estimated that the time needed to detect these lines at the 3σ level is 2 days for the 511 keV line and 8 days for the 1809 keV line.

Acknowledgements

It is a pleasure to thank Scott Barthelmy, Jeff DuMonthier, Ron Harten, Manny Karageorge, Ron Murphy, Sam Pascarrelli, Maggie Rilling, Larry Scott, and Jack Tueller for valuable contributions. AO acknowledges an NAS/NRC Resident Research Associateship.

References

Fenimore, E. E., Laros, J. G., Klebesadel, R. W., Stockard, R. E., and Kane, S. R.: 1981, 'Gamma-Ray-Transients and Related Phenomena', *AIP Conference Proceedings* **77**, 201.

Fenimore, E. E., Klebesadel, R. W., and Laros, J. G.: 1983, *Adv. Space Res.* **3**(4), 1983.

Evenson, P.: 1987, in G. E. Kocharov (ed.), *Observation of Solar Flare Neutron Decay Protons*, Proc. Moscow Solar Neutron Workshop, Ioffe Institute, Leningrad.

Gehrels, N.: 1985, *Nucl. Instr. Meth.* **A239**, 324.

Heuter, G. J. and Gruber, D. E.: 1982, in W. Brinkman and J. Trumper (eds.), *Accreting Neutron Stars*, MPI Garching, Munich, p. 213.

Hurley, K.: 1989a, in M. Shapiro and J. Wefel (eds.), *Cosmic Gamma-Ray Bursts and Cosmic Neutrinos*, D. Reidel Publ. Co., Dordrecht, Holland.

Hurley, K.: 1989b, *Proc. 14th Texas Symposium on Relativistic Astrophysics, Annals of the New York Academy of Sciences* **571**, 442.

Klebesadel, R. W., Strong, I. B., and Olsen, R. A.: 1972, *Astrophys. J.* **182**, L85.

Kouveliotou, C., Desai, U. D., Cline, T. L., Dennis, B. R., Fenimore, E. E., Klebesadel, R. W., and Laros, J. G.: 1988, *Astrophys. J.* **330**, L101.

Lin, R. P., Schwartz, R. A., Kane, S. R., Pelling, R. M., and Hurley, K. C.: 1984, *Astrophys. J.* **283**, 421.

Lingenfelter, R. E. and Ramaty, R.: 1989, *Astrophys. J.* **343**, 686.

Mazets, E. P., Golenetskii, S. V., Ilynskii, V. N., Aptekar, R. L., and Guryan, Yu. A.: 1979, *Nature* **282**, 587.

Mazets, E. P., Golenetskii, S. V., Aptekar, R. L., Guryan, Yu. A., and Ilynskii, V. N.: 1981, *Nature* **290**, 278.

Mayer-Hasselwander, H. A. *et al.*: 1980, *Proc. 9th Texas Symposium on Relativistic Astrophysics, Annals of the New York Academy of Sciences* **336**, 211.

Meegan, C. A. *et al.*: 1992, *Nature* **355** 234.

Murakami, T. M. *et al.*: 1988, *Nature*, **335**, 234.

Niel, M., Jourdain, E., and Roques, J. P.: 1990, *Astron. Astrophys.* **228**, L1.

Nolan, T.: 1990a, *Networking with Net Bios, LAN Technology* **6**, 42.

Nolan, T.: 1990b, *Real Time Data Acquisition Using DMA, Dr Dobb's Journal* **15**, 28.

Owens, A., Bhattacharya, D., and Sembay, S.: 1990, *Astrophys. J.* **352**, 741.

Owens, A. *et al.*: 1991, *IEEE Trans. Nucl. Sci.* **38**, 559.

Paciesas, W. S., Cline, T. L., Teegarden, B. J., Tueller, J., Durouchoux, P., and Hameury, J. M.: 1982, *Astrophys. J.* **260**, L7.

Paul, J. *et al.*: 1991, in Ph. Durouchoux and N. Prantzos (eds.), *Proc. of the Symposium on Gamma-Ray Line Astrophysics*, Publ. AIP, New York, in press.

Peterson, L. E., Gruber, D. E., Matteson, J. L., and Vette, J. E.: 1970, *Environment Research Satellite-18 Data Reduction and Analysis*, UCSD-SP-70-03, p. 83.

Ramaty, R.: 1986, in Peter A. Sturrock (ed.), *Physics of the Sun*, D. Reidel Publ. Co., Dordrecht, Holland.

Teegarden, B. J. and Cline, T. L.: 1980, *Astrophys. J.* **236**, L67.

Teegarden, B. J. *et al.*: 1992, *Proceedings of the Compton GRO Symposium*, St. Louis.

Wood, K. S., Byam, E. T., Chubb, T. A., Friedman, H., Meekins, J. F., Share, G. H., and Yentis, D. J.: 1981, *Astrophys. J.* **247**, 632.

Vestrand, W. T., Chupp, E. L., Rieger, E., and Share, G. H.: 1987, *Astrophys. J.* **332**, 1010.